Earth and Planetary Science Letters 425 (2015) 204–218

Contents lists available at ScienceDirect

Earth and Planetary Science Letters

www.elsevier.com/locate/epsl

The growth of a mountain belt forced by base-level fall: Tectonics and surface processes during the evolution of the Alborz Mountains, N Iran

Paolo Ballato [a,*], Angela Landgraf [a], Taylor F. Schildgen [a], Daniel F. Stockli [b], Matthew Fox [c,d], Mohammad R. Ghassemi [e], Eric Kirby [f], Manfred R. Strecker [a]

[a] *Institut für Erd- und Umweltwissenschaften, Universität Potsdam, 14476 Potsdam, Germany*
[b] *Department of Geological Sciences, Jackson School of Geosciences, Austin, TX 78712, USA*
[c] *Department of Earth and Planetary Science, University of California, Berkeley, CA, USA*
[d] *Berkeley Geochronology Center, Berkeley, CA, USA*
[e] *Research Institute for Earth Sciences, GSI, Tehran 13185-1494, Iran*
[f] *College of Earth, Ocean, and Atmospheric Sciences, Oregon State University, Corvallis, OR 97331-5503, USA*

ARTICLE INFO

Article history:
Received 3 March 2015
Received in revised form 26 April 2015
Accepted 28 May 2015
Available online 12 June 2015
Editor: A. Yin

Keywords:
orogenic processes
surface processes
base-level fall
erosion
rock uplift
knickpoints

ABSTRACT

The idea that climatically modulated erosion may impact orogenic processes has challenged geoscientists for decades. Although modeling studies and physical calculations have provided a solid theoretical basis supporting this interaction, to date, field-based work has produced inconclusive results. The central–western Alborz Mountains in the northern sectors of the Arabia–Eurasia collision zone constitute a promising area to explore these potential feedbacks. This region is characterized by asymmetric precipitation superimposed on an orogen with a history of spatiotemporal changes in exhumation rates, deformation patterns, and prolonged, km-scale base-level changes. Our analysis suggests that despite the existence of a strong climatic gradient at least since 17.5 Ma, the early orogenic evolution (from ∼36 to 9–6 Ma) was characterized by decoupled orographic precipitation and tectonics. In particular, faster exhumation and sedimentation along the more arid southern orogenic flank point to a north-directed accretionary flux and underthrusting of Central Iran. Conversely, from ∼6 to 3 Ma, erosion rates along the northern orogenic flank became higher than those in the south, where they dropped to minimum values. This change occurred during a ∼3-Myr-long, km-scale base-level lowering event in the Caspian Sea. We speculate that mass redistribution processes along the northern flank of the Alborz and presumably across all mountain belts adjacent to the South Caspian Basin and more stable areas of the Eurasian plate increased the sediment load in the basin and ultimately led to the underthrusting of the Caspian Basin beneath the Alborz Mountains. This underthrusting in turn triggered a new phase of northward orogenic expansion, transformed the wetter northern flank into a new pro-wedge, and led to the establishment of apparent steady-state conditions along the northern orogenic flank (i.e., rock uplift equal to erosion rates). Conversely, the southern mountain front became the retro-wedge and experienced limited tectonic activity. These observations overall raise the possibility that mass-distribution processes during a pronounced erosion phase driven by base-level changes may have contributed to the inferred regional plate-tectonic reorganization of the northern Arabia–Eurasia collision during the last ∼5 Ma.

© 2015 Elsevier B.V. All rights reserved.

1. Introduction

Since the first suggestion that erosion can dictate the internal dynamics of orogenic wedges (Davis et al., 1983), numerous analogue experiments (e.g., Koons, 1990; Hoth et al., 2006), numerical simulations (e.g., Willett et al., 1993; Willett, 1999), and analytical solutions to orogenic-wedge models (e.g., Whipple and Meade, 2006) have shown that erosion of a tectonically active orogen may affect deformation processes in two ways: 1) shifting deformation outward into the foreland or internally within the wedge to maintain a critical orogenic taper (e.g., Davis et al., 1983; Willett et al., 1993); and 2) focusing rock uplift in areas of high precipitation, where erosional processes are thought to be more efficient (e.g., Willett, 1999; Thiede et al., 2004; Hodges et al., 2004; Reiners and Brandon, 2006). While the first mechanism has proven difficult to demonstrate with field data

* Corresponding author.
E-mail address: ballato@geo.uni-potsdam.de (P. Ballato).

http://dx.doi.org/10.1016/j.epsl.2015.05.051
0012-821X/© 2015 Elsevier B.V. All rights reserved.

(for a review see Whipple, 2009), spatial correlations between long- to short-term erosion rates and modern mean-annual precipitation in some orogenic systems have been presented as proof of a coupling among erosion (which is thought to be controlled by climate, although such a linkage is not yet fully understood; e.g., DiBiase and Whipple, 2011), topography, and tectonics. Examples of such an interplay include the Washington Cascades (e.g., Reiners and Brandon, 2006), the Southern Alps of New Zealand (e.g., Koons, 1990), the central and southern sectors of the eastern central Andes (e.g., Bookhagen and Strecker, 2012), and the southern Greater Himalaya (e.g., Hodges et al., 2004). Nonetheless, in nearly every orogen where a coupling between climate and tectonics has been proposed, alternative data sets and interpretations have argued against it, especially for large orogens with high heat flow, such as the Himalaya (e.g., Burbank et al., 2003) and the Andes (e.g., Gasparini and Whipple, 2014).

Here, we explore the external controls on orogeny in the Alborz Mountains, the deforming intracontinental orogen related to the Arabia–Eurasia collision zone (Fig. 1). According to GPS data and absolute gravity measurements, the northernmost deformation front accommodates ∼85% (∼6 mm/yr) of the current total shortening across the range along the Caspian Fault (also known as the Khazar Fault) coupled with surface uplift rates of 1 to 5 mm/yr (Fig. 1; Djamour et al., 2010). Ongoing deformation therefore appears to be concentrated along the northern orogenic margin, as shown by the distribution of shallow crustal seismicity (e.g., Tatar et al., 2007; Donner et al., 2013). Furthermore, the orogen forms an effective barrier to rainfall, with the northern flank receiving up to 2 m/yr sourced from the Caspian Sea, and an arid to semiarid southern flank receiving <0.5 m/yr (Fig. 1). Elevated topography of the range has existed at least since the Eocene, as documented by regional stratigraphic relationships (e.g., Guest et al., 2006a; Rezaeian et al., 2012), while a stable C and O pedogenic isotope record documents a climatic gradient across the range since at least 17.5 Ma (Ballato et al., 2010). In contrast, apatite fission track and zircon (U–Th)/He thermochronometers (Fig. 2; Guest et al., 2006b; Rezaeian et al., 2012; Ballato et al., 2013) do not illustrate any long-term asymmetry in exhumation rates, as expected in active orogens characterized by orographic precipitation (e.g., Willett, 1999). Taken together, these observations suggest that if a present-day coupling among active deformation, topography, and erosional processes (through orographic precipitation) indeed exists, it must have been established relatively recently.

To reconcile these apparently contrasting observations and to explore what mechanisms have dictated orogenic evolution, we combine analyses of river-channel morphology and new apatite and zircon (U–Th)/He cooling ages with published information, including low-temperature thermochronology data (Axen et al., 2001; Guest et al., 2006b; Rezaeian et al., 2012; Ballato et al., 2013), basin-fill histories from the southern Alborz foreland (Ballato et al., 2008), the Caspian Sea (e.g., Allen et al., 2002; Brunet et al., 2003; Green et al., 2009), and the intermontane Taleghan-Alamut basin (Guest et al., 2007), long-term paleoclimatic records (Ballato et al., 2010), and decadal erosion rates (Rezaeian, 2008). Using these data, we document temporal shifts in the locus of active deformation and exhumation across the orogen, and compare them to both long-term and modern climate records to evaluate possible feedbacks among tectonics, climate, and topography. Furthermore, we consider how the km-scale base-level drop of the Caspian Sea between ∼6 and 3.2 Ma (Forte and Cowgill, 2013; Van Baak et al., 2013) may have influenced the orogenic evolution of the Alborz and potentially also other mountain belts surrounding the Caspian.

2. Geologic setting

The Alborz Mountains of northern Iran are an intracontinental, double-verging orogen within the Arabia–Eurasia collision zone, located between the relatively stable South Caspian Basin and Central Iranian Block (Fig. 1; e.g., Allen et al., 2004). Currently, the northern margin of the central western Alborz range accommodates oblique plate convergence through a combination of shortening (∼6 mm/yr) and left-lateral wrenching (∼2 mm/yr), while deformation rates along the southern flank are <1 mm/yr (shortening) to ∼1 mm/yr (left-lateral wrenching; Fig. 1; Djamour et al., 2010). Although sparse, seismicity appears to corroborate this pattern (Tatar et al., 2007; Aziz Zanjani et al., 2013; Donner et al., 2013; Nemati et al., 2013).

Deformation in the Alborz Mountains has led to more than 50 km of shortening (Guest et al., 2006a), thickened crust of up to 55 km (e.g., Motavalli Anbaran, et al., 2011), and the growth of high topography with several peaks >4 km (Fig. 1). The highest peak is the ∼6-km-high, Quaternary Damavand volcano, located in the orogen interior, which is also the locus of the present-day rainfall maximum (Fig. 1).

The tectonic history of the orogen involves multiple contractional and extensional phases (e.g., Allen et al., 2003; Guest et al., 2006b). The last significant extensional/transtensional phase occurred during the Eocene, and was associated with the deposition of up to 7 km of volcanoclastic sediments along the southern orogenic flank (e.g., Ballato et al., 2013). Conversely, shallow-water marine deposits along the northern orogenic flank reflect shelfal sedimentation in the southern Caspian Sea (Fig. 2). This depositional history suggests that the Alborz range comprised a paleotopographic high, and hence, the occurrence of Mesozoic and older rocks along the northern orogenic flank does not reflect greater late Cenozoic exhumation, but rather a different pre-Miocene paleo-geographic history.

Data from associated sedimentary basins (Guest et al., 2007; Ballato et al., 2008, 2011), structural and geomorphic analysis (Allen et al., 2003; Guest et al., 2006a; Zanchi et al., 2006; Landgraf et al., 2009), and low-temperature thermochronology (Fig. 2; Axen et al., 2001; Guest et al., 2006b; Rezaeiean et al., 2012; Ballato et al., 2013) document that shortening started during the Eo-Oligocene, possibly during the early stages of continental collision, and accelerated diachronously across different structures by ∼20–18 Ma, most likely in response to changes in plate coupling (Ballato et al., 2011). The last pulse of deformation and related exhumation occurred since ∼6 to 3 Ma. It has been mostly attributed to either a regional plate-tectonic reorganization (Axen et al., 2001; Allen et al., 2004) or a climatically induced intensification of erosion during the Pliocene Caspian Sea isolation (Rezaeian et al., 2012).

3. Methods

3.1. Zircon and apatite (U–Th)/He thermochronology

To improve our knowledge about the spatiotemporal evolution of exhumation along the southern flank of the central Alborz Mountains, we present 12 new apatite (U–Th)/He (AHe, closure temperature of ∼60 °C; e.g., Farley, 2000) and 7 new zircon (U–Th)/He (ZHe, closure temperature of ∼180 °C; e.g., Wolfe and Stockli, 2010) cooling ages. For ZHe thermochronology, three single-grain aliquots per sample were analyzed following the protocol of Wolfe and Stockli (2010). For AHe thermochronology, we analyzed at least three double-grain aliquots per sample following Farley (2000). Laboratory measurements were performed at the Isotope Geochemistry Laboratory of the University of Kansas. (U–Th)/He ages were calculated using the standard age equation

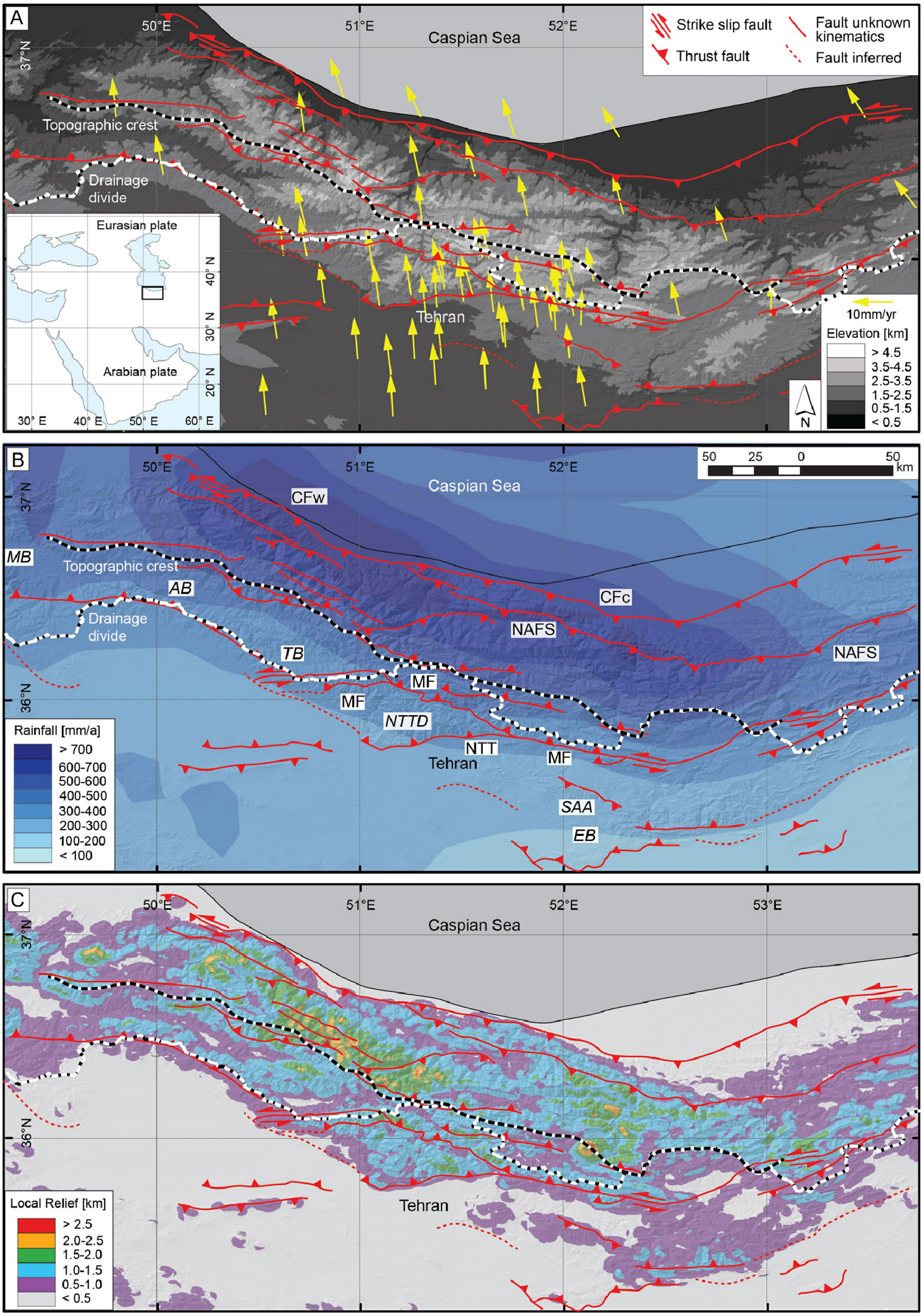

Fig. 1. (A) Digital elevation model (DEM) of the Alborz Mountains (see inset for location) with GPS velocities from Djamour et al. (2010) with respect to stable Eurasia (B) Annual rainfall data based on TRMM 3B42 estimates from 1998 to 2007 (B. Bookhagen, pers. commun.). Although TRMM data appear to underestimate rainfall values collected in rain gauge stations (Javanmard et al., 2010), the pattern of precipitation highlights the pronounced orographic rain-shadow effects across the Alborz Mountains. Abbreviations: NTT, North Tehran Thrust; MF, Mosha Fault; NAFS, North Alborz Fault; CF, Caspian Fault (w, western; c central segments); *NTTD*, North Tehran Transpressional Duplex; *SAA*, Southern Alborz Anticline; *EB*, Eyvanekey Basin; *AB*, Alamut Basin; *TB*, Taleghan Basin, *MB*, Manjil Basin. (C) Local relief map over a 2.0 km radius; note that higher relief areas in the central western Alborz Mountains are mostly along the northern orogenic flank. (For interpretation of the colors in this figure, the reader is referred to the web version of this article.)

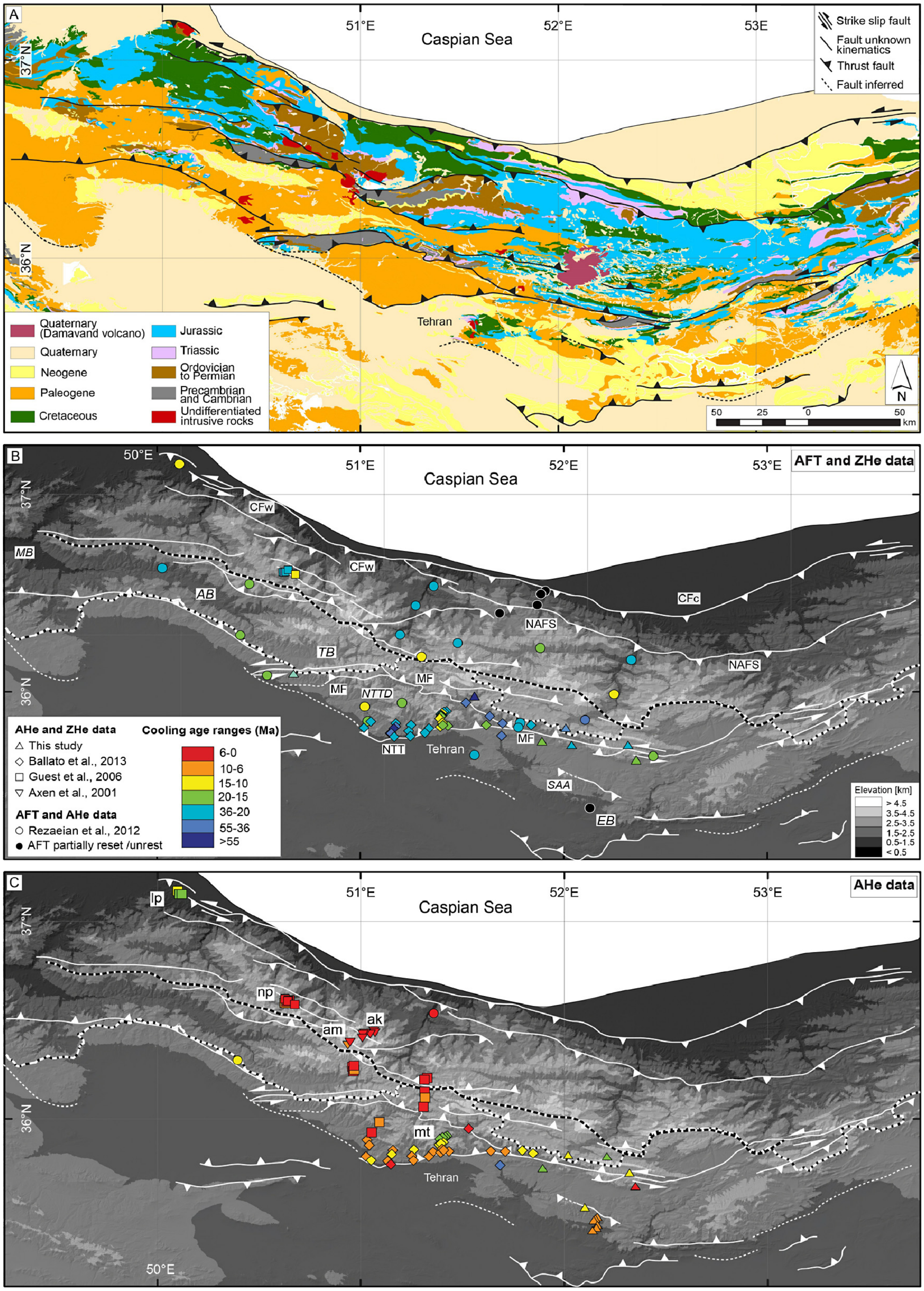

Fig. 2. (A) Simplified geologic map of the Alborz Mountains based on 1:250.000 quadrangle maps of the Geological Survey of Iran (see Ballato et al., 2013 and references therein). (B) DEM with Apatite Fission Track (AFT) and Zircon (U–Th)/He (ZHe) cooling ages, and (C) Apatite (U–Th)/He (AHe) cooling ages (see legend for the data source). Note the only AFT are from Rezaian et al. (2012). Abbreviations used in C include outcrop locations such as: lp, Lalijan Pluton, np, Nusha Pluton; ak, Akapol Pluton; am, Alam Kuh Pluton; mt, Mount Tochal; KB, Kond Basin and EB, Eyvanekey Basin. (For interpretation of the colors in this figure, the reader is referred to the web version of this article.)

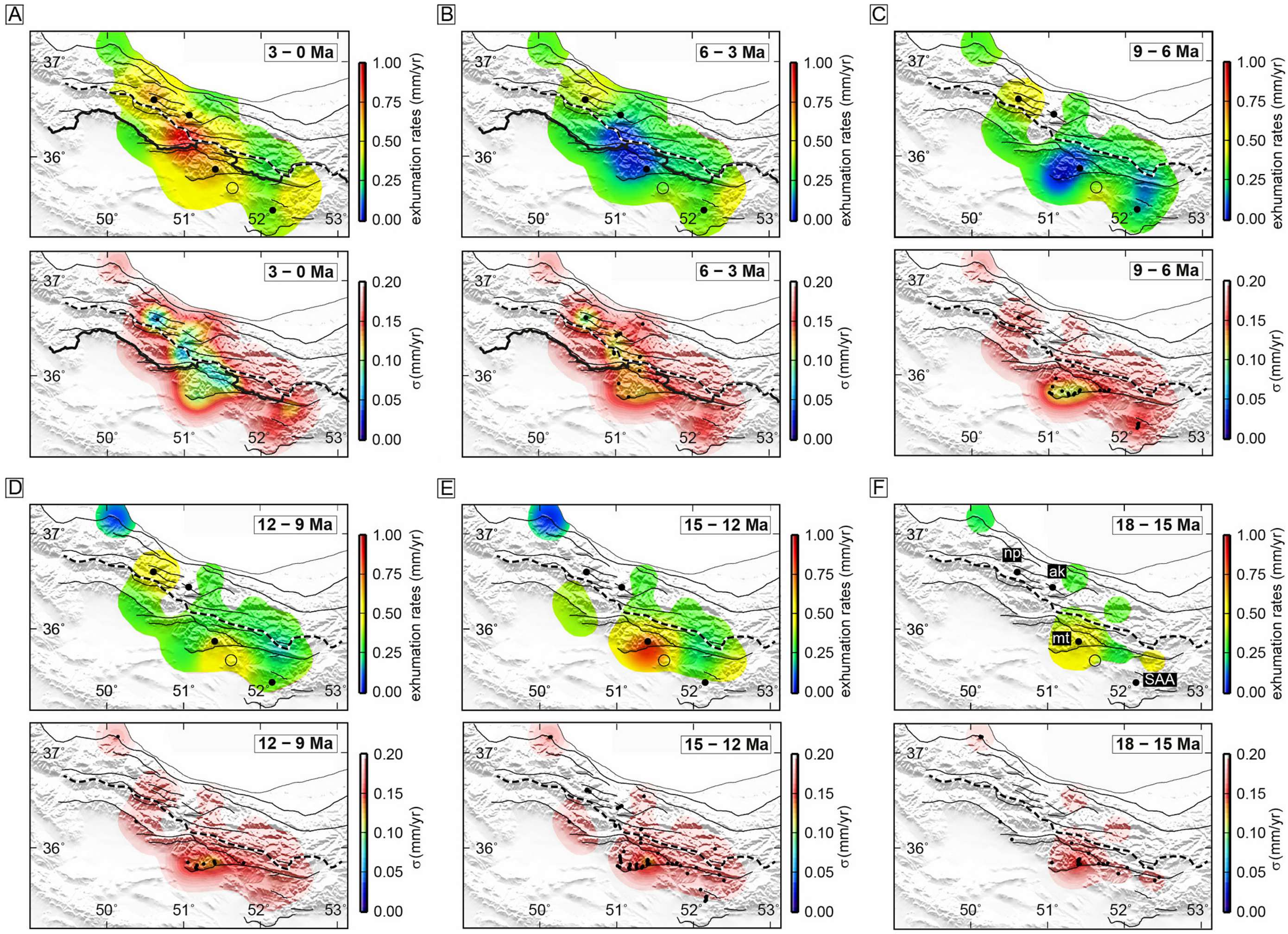

Fig. 3. (A to F) Exhumation rate history from the linear inversion method from 18 Ma to present for 3 Myr time windows (upper panels) and associated errors (σ, lower panels). The four large black dots of each upper panel represent the sites used for deriving the exhumation rate history shown in Fig. 4, while the small black dots of each lower panels show the location of samples used for the calculation for that specific time window. The circles in each upper panel indicate the location of the borehole from which the modern geothermal gradient was measured (Sass et al., 1971). The major faults are indicated with thin black lines, while the topographic crest (figures B to F) and the drainage divide (figures A and B) are shown as thick dashed and solid line. (For interpretation of the colors in this figure, the reader is referred to the web version of this article.)

and applying FT corrections assuming homogeneous U and Th distribution (Farley et al., 1996). Age uncertainties (2σ) reflect the reproducibility of replicate analyses of laboratory-standard samples and comprise ~6% for apatite and ~8% for zircon ages. Our new data are plotted together with published cooling ages (Fig. 2). The complete dataset is provided in the supplementary information.

3.2. Linear inversion of thermochronological data

The combination of our new and previously published data comprises a total of 75 AHe, 26 apatite fission track (AFT), and 43 ZHe cooling ages, enabling us to constrain exhumation rates over the last 18 Ma. To infer exhumation rates, we apply a linear inverse method, which is designed to exploit exhumation-rate constraints from age-elevation relationships and from multiple thermochronometric systems with different closure temperatures (Fox et al., 2014).

Here, we used a prior exhumation rate of 0.4 ± 0.2 km/Myr, a correlation length scale of 25 km, and a time-step length of 3 Myr. The thermal model was calibrated to produce modern geothermal gradients of 25 °C/km at the location of a borehole immediately east of Tehran (Sass et al., 1971). As the resolution of our results (divided into 3 million-year time windows) decreases significantly back in time, we focus on exhumation rates for time intervals younger than 18 Ma (Fig. 3). The exact values of the inferred exhumation rates are expected to be sensitive to the time-step length and thus the uncertainty associated with the exhumation-rate estimate is also model dependent. Therefore, we only discuss aspects of the results that are robust with respect to model parameterization. In particular, in Fig. 4 we show the sensitivity of inferred exhumation rates and model uncertainty (σ) as a function of time-step length (with timesteps of, 1 3, 5 and 10 Myr), for four localities along the northern (Nusha and Akapol plutons) and southern (Mount Tochal and Southern Alborz anticlines) orogenic flank.

3.3. River-channel steepness analysis

The morphology of fluvial networks can reflect external forcing on landscape evolution (i.e., rock uplift, eustasy, drainage-pattern reorganization, and climate; e.g., Kirby and Whipple, 2012) and ultimately the dynamic feedbacks among topography, climate, and tectonics at an orogenic scale (e.g., Whipple, 2009; Gasparini and Whipple, 2014). Empirical data show that a power-law scaling exists between channel slope and contributing drainage area, and rock-uplift rate appears to exert a first-order control on this relationship (e.g., Whipple and Tucker, 1999). Therefore, at steady

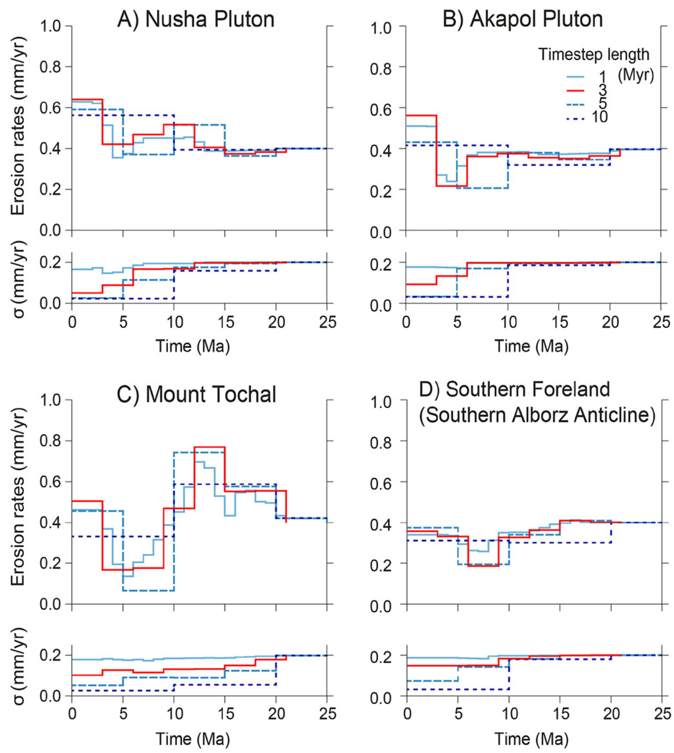

Fig. 4. Exhumation histories from the northern (A–B, Nusha and Akapol plutons) and the southern (C–D, Mount Tochal, North Tehran Transpressional Duplex and Southern Alborz Anticline in southern Miocene foreland) orogenic flank for four different time steps (1, 3, 5 and 10 Myr) and associated uncertainty (σ). (For interpretation of the colors in this figure, the reader is referred to the web version of this article.)

state, the river steepness (k_{sn}, slope normalized by upstream drainage area raised to a specified concavity index) should correlate with rock-uplift rate, and in the absence of climate-tectonic coupling, is anti-correlated with erodibility (a function of regional precipitation trends and lithology). We extracted k_{sn} values from 90-m resolution SRTM (Shuttle Radar Topography Mission) data using the Stream Profiler tool (http://www.geomorphtools.org/; Wobus et al., 2006). The river network was automatically analyzed using a 1-km smoothing window with 20-m contour intervals and a reference concavity of 0.45 (e.g., Kirby and Whipple, 2012). Our k_{sn} analysis does not include the upper reaches of the Alam Kuh pluton in the central Alborz Mountains (Figs. 2 and 3), which is the only location in the region significantly influenced by glacial erosion. The results of the river-channel steepness analysis are reported and illustrated in Figs. 4 and 5, and in the supplementary information.

4. Results

4.1. New low-temperature thermochronology data

The cooling ages exhibit relatively good reproducibility, with five ZHe (out of seven) and five AHe (out of six) cooling ages representing an average of three aliquots with overlapping uncertainties (see supplementary material). These samples have depositional ages older than Oligocene. Additional AHe data from Oligo-Miocene sandstones collected in the southern foreland (Southern Alborz Anticline) have a lower reproducibility and only two out of six cooling ages represent an average of three aliquots. The aliquots discarded for the mean age calculation exhibit cooling ages older than (or similar to) the depositional age.

Based on their structural location, the samples can be subdivided into three groups: the hanging wall of the Mosha Fault, its footwall, and the Southern Alborz Anticline (Fig. 2). The hanging wall of the Mosha Fault is characterized by four ZHe cooling ages of ∼65 to 30 Ma and three AHe ages of 16 to 13 Ma, while its footwall yields three ZHe ages of ∼32 to 16 Ma and two AHe ages of 17 to 5 Ma. Samples from the Southern Alborz Anticline include one from Eocene volcanics with an AHe cooling age of 13.4 ± 0.8 Ma in the core of the fold, while sandstone samples along its southern flank (deposited in the southern foreland basin) yield six AHe ages ranging from 6.9 ± 0.4 to 8.5 ± 0.5 Ma.

4.2. Spatiotemporal pattern of exhumation rates

Our linear inversion of thermochronology data includes samples collected along the southern orogenic flank (Eocene to Miocene volcanic rocks, volcanoclastic and sedimentary rocks) and samples from the axial part and the northern flank (either Paleozoic and Mesozoic sedimentary rocks, or relatively small intrusive bodies) (Fig. 2). In the discussion that follows, we define the "northern flank" and "southern flank" as relative to the topographic crest (Figs. 1, 2, and 3).

From 18 to 9 Ma, the southern orogenic flank was characterized by moderate exhumation rates in the hanging wall and footwall of the Mosha Fault (∼0.8 to 0.3 mm/yr, Figs. 3 and 4). From 9 Ma, exhumation rates along the North Tehran Transpressional Duplex (southern flank) started to decrease, reaching minimum values of 0.1 mm/yr between 6 and 3 Ma (Figs. 3 and 4). To the east, the pattern is less resolved, however, it also seems that exhumation rates started decreasing from 9 Ma. In contrast, the northern flank experienced gradually increasing exhumation rates since ∼12 Ma (from ∼0.2 to ∼0.4 mm/yr, although the resolution for the northern flank is limited until ∼6 Ma. The exhumation rates along the northern flank may have experienced a slight decrease from 6 to 3 Ma, but it was still eroding faster than the southern flank (Figs. 3 and 4). Finally, exhumation rates during the last 3 Ma increased along both orogenic flanks up to 0.3–0.6 mm/yr, with maximum values in the axial zone (0.8 mm/yr; Fig. 3). These exhumation rates averaged over the last 3 Ma are similar to those obtained from suspended sediment concentrations measured at gauging stations (0.2 to 0.6 mm/yr) for a time interval of 10 to 55 years (Rezaeian, 2008).

4.3. River-channel morphology

The north-draining rivers flow into the Caspian Sea, whose modern base level is about 27 meters below sea level. The longer rivers reach into the axial orogenic sectors, while the short frontal streams drain only the northern flank (Fig. 5). Both drainage systems are associated with high relief and high mean annual precipitation, and exhibit generally high normalized steepness indices (k_{sn}). These steepened sections of the channels are often associated with pronounced knickpoints or transition zones that do not coincide with any apparent lithological contacts (see supplementary information), except across the hanging wall of some fault segments located in the interior of the orogen (Figs. 4 and 5). This pattern implies the channels are characterized by several transient knickpoints, reflecting either a change in tectonic (rock-uplift rate) or climatic (erosion rate) forcing, or base-level fall (Whipple and Tucker, 1999; Kirby and Whipple, 2012). High k_{sn} values occur also around the ∼600-kyr-old (Davidson et al., 2004) Damavand Volcano (Fig. 5). In the eastern orogenic sectors, k_{sn} values of north-draining channels are lower than those in the west and tend to increase only toward the high-relief sectors of the axial zone (Fig. 5). The pattern of k_{sn} values along the central western sectors of the northern flank correlates positively with rainfall maxima.

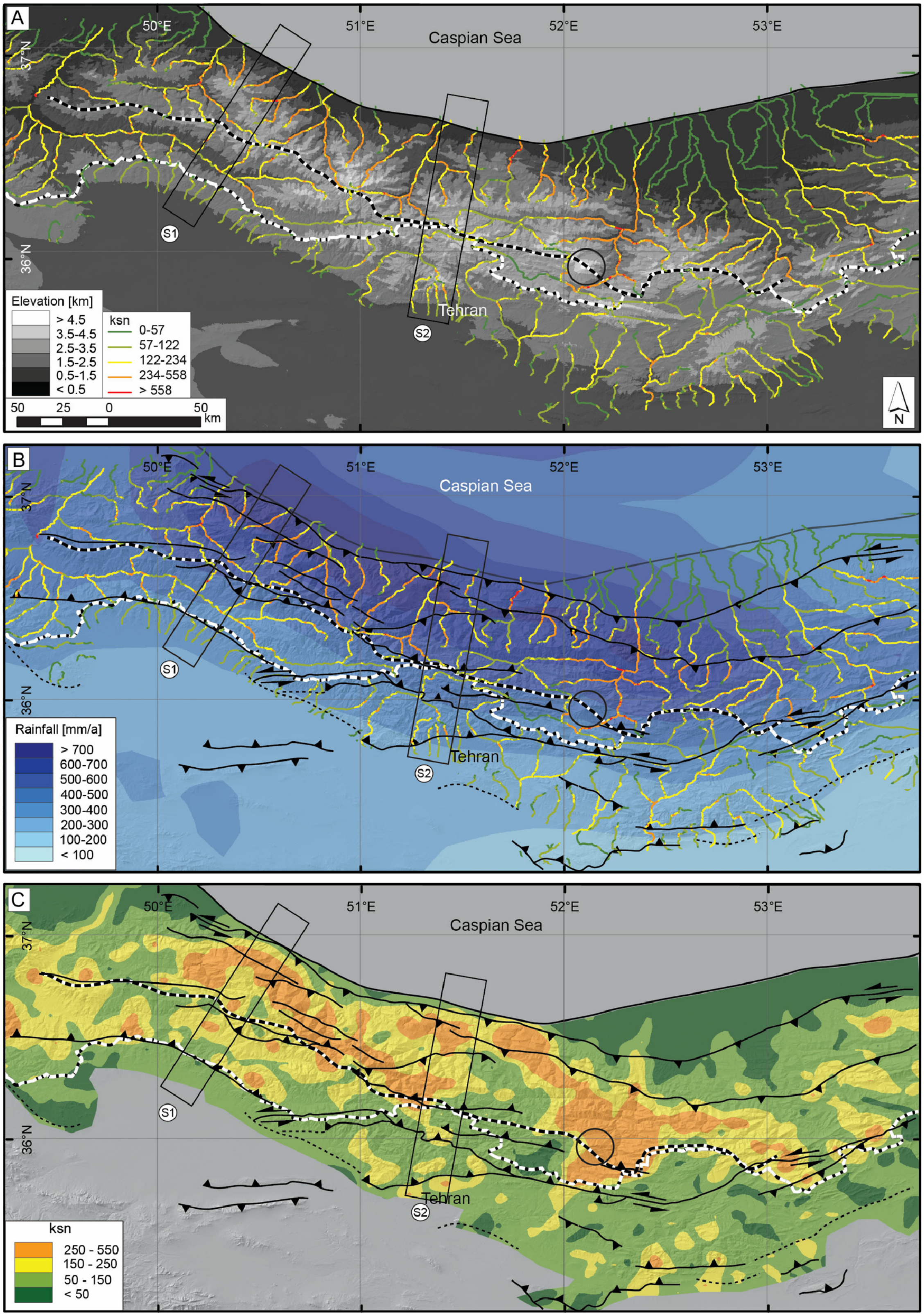

Fig. 5. (A) DEM and (B) annual rainfall map with streams color-coded according to their normalized river-steepness index (k_{sn}). Note that high k_{sn} values are located along the northern orogenic flank. The black boxes show the location of the swath profiles of Fig. 8; box S2 shows also the approximate position of the crustal scale profile of Fig. 7. (C) Interpolated map of normalized steepness index (k_{sn}) values, which to a first approximation (in the absence of significant variations in erosivity) are interpreted to reflect spatial variations in rock uplift rate. The circle shows the location of the Damavand Volcano. (For interpretation of the colors in this figure, the reader is referred to the web version of this article.)

The south-draining rivers flow into the playa lakes of Central Iran, whose base levels are at 700 to 800 m elevation. These rivers are characterized by relatively low k_{sn} values and few, indistinct knickpoints (Fig. 5). The highest k_{sn} values are located in the high-relief area north of Tehran and locally around the south-eastern sector of the orogenic bend of the Alborz.

Finally, the range comprises several transverse river basins subparallel to the structural trend that drain former Mio-Pliocene intermontane basins and flow into the Caspian Sea (Fig. 2; Guest et al., 2007). These transverse channels generally have low k_{sn} values (Fig. 5).

5. Orogenic evolution of the Alborz Mountains

Our combination of new and published data provides the basis for reconstructing the spatiotemporal evolution of the Alborz Mountains. Below, we summarize the data documenting the orogenic evolution for three time intervals between ∼36 to 6, ∼6 to 3, and ∼3 to 0 Ma.

5.1. Oligo-Miocene (∼36 to 6 Ma) orogenic evolution

A number of previous studies and our new data document late Cenozoic outward orogenic expansion of the Alborz Mountains. After an early phase of crustal shortening, which led to the growth of the axial range starting approximately at the Eo-Oligocene boundary (Ballato et al., 2011; Rezaeian et al., 2012), the southern range front migrated southward. Enhanced exhumation occurred through the propagation of the deformation front in the footwall of the Mosha Fault and the development of the North Tehran Transpressional Duplex by ∼18 Ma (Ballato et al., 2013; Landgraf et al., 2013; Figs. 2, 3 and 4). Early to middle Miocene outward orogenic expansion was marked by enhanced foreland-basin subsidence along the southern flanks of the range (Ballato et al., 2008), sedimentary facies retrogradation, and changes in sediment composition, indicating unroofing and/or drainage reorganization during sustained tectonic activity (Ballato and Strecker, 2014). Final basin uplift and erosion occurred during the propagation of the deformation front ∼30 km into the southern foreland, as indicated by the widespread progradation of coarse-grained sedimentary facies (Ballato et al., 2008) and sediment provenance data (Ballato et al., 2011).

Outward propagation of deformation may have also occurred in the northwestern Alborz Mountains associated with exhumation of the hanging wall of the western Caspian Fault, at rates of ∼0.2 to 0.3 mm/yr (Figs. 3 and 4). These exhumation and deformation patterns imply that by middle Miocene time, the central–western Alborz range had reached a lateral extent similar to the present-day, with the North Tehran Thrust and the western Caspian Fault forming the southern and northernmost frontal faults, respectively (Figs. 2 and 3). From 9–6 Ma (or possibly even earlier), however, a decrease in exhumation rates along the southern orogenic flank relative to the northern one occurred, suggesting either a change in either climate that affected erosional processes or in tectonic boundary conditions. While the lack of high-precision paleoclimate data does not allow testing in detail the influence of climate on erosion over this timeframe, the latter hypothesis will be discussed in Section 6.4.

5.2. Orogenic evolution between 6 and 3 Ma

After the initial phase of mainly southward-directed growth of the Alborz Mountains, the pattern of exhumation and deformation changed, as indicated by the thermochronometric data. In particular, along the southern orogenic flank, exhumation rates that had already started decreasing between 9 and 6 Ma reached minimum values between 6 and 3 Ma (Figs. 3 and 4), implying that tectonic exhumation had largely ceased. Exhumation during that time interval was instead localized along the northern orogenic flank and within the western axial sectors. However, only limited total exhumation was accommodated by the major faults along the northern mountain front, as illustrated by the ∼17–13 Ma AHe and Oligocene or older (partially reset) AFT cooling ages in the hanging wall of the western Caspian Fault and the North Alborz Fault (Fig. 2). Combined, these results document that most of the erosion occurred within catchments drained by northern rivers (Fig. 3), and that the locus of fault-related exhumation should have stepped backward into the orogen interior and toward its northern orogenic flank. Enhanced exhumation in the western axial zone between 6 and 3 Ma is also documented by subhorizontal, poorly dated Plio-Pleistocene conglomerates, covering fine-grained, deformed Miocene strata within the eastern sectors of the Taleghan and Alamut intermontane basins (Fig. 2; Guest et al., 2007).

5.3. Orogenic evolution from 3 Ma to the present

Following Caspian Sea level rise at ∼3.2 Ma at least up to the modern western Caspian Sea coast line (Van Baak, et al., 2013), the growth of new segments of the Caspian Fault along the central–eastern Alborz range documents northward orogenic expansion (Fig. 2). Although the depositional age of the synorogenic sediments of the southern Caspian Basin is poorly constrained, the eastern Caspian Fault seems to have incorporated Pliocene sediments into the growing orogenic wedge (Berberian, 1983). Based on correlations between onshore and offshore data, Berberian (1983) suggested a minimum throw of 3 km along the central eastern Caspian Fault during the last 2 to 4 Myr. In the central western Alborz the increase in exhumation rates seems to be associated with renewed faulting along the western Caspian Fault (Fig. 3).

An increase in shortening rates (and uplift) along the northern flank of the orogen is supported by high normalized channel steepness indices (k_{sn}) bounded by knickpoints upstream (Figs. 4 and 5). Within the central eastern Alborz range, where exhumation rates increased from ∼0.35 to 0.5 mm/yr at ∼3 Ma (Fig. 3), a knickpoint associated with the increase in uplift rate should occur at ∼450 m elevation (see supplementary material). In the central western Alborz, where exhumation rates increased from ∼0.2–0.35 to 0.3–0.6 mm/yr, tectonically generated knickpoints should occur at ∼750 to 900 m elevation (see supplementary material). Although it is difficult to link the numerous small knickpoints along the river profiles to distinct tectonic events, their existence (with most of them at elevations of ∼400 to 1400 m) corroborates an overall increase in tectonic activity and exhumation over the last 3 Myr.

Active deformation along the northern orogenic flank also agrees with recent drainage-network evolution (Ghassemi, 2005) and geodetic data, documenting that in the central western Alborz Mountains, present-day oblique strain is partitioned into shortening (6 mm/yr) and left-lateral wrenching (2 mm/yr) across the northernmost deformation front (Caspian Fault), while the southern flank accommodates shortening at <1 mm/yr (Fig. 1; Djamour et al., 2010). For a 35–30° dip of the Caspian Fault (e.g., Tatar et al., 2007; Donner et al., 2013) and 6 mm/yr of horizontal shortening, underthrusting of the Caspian Basin beneath the Alborz Mountains would occur at a rate of 6.9 mm/yr ($6/\cos 30°$), implying 3.5 mm/yr of crustal thickening along the northern orogenic flank (i.e., $6 \times \tan 30°$; Fig. 6). Assuming Airy isostatic equilibrium with a mean crustal density of 2.75–2.85 kg/m^3 and mantle density of 3.2–3.3 kg/m^3, rock uplift rates along the northern flank would be 0.4 to 0.7 mm/yr. 3-D numerical boundary-element modeling of the vertical displacement field (Landgraf et al., 2013 and references therein) across the Caspian Fault allows us to estimate the spatial distribution of rock-uplift rates along the northern orogenic flank resulting from shortening along the Caspian Fault (Fig. 8). The calculation is based on fault interaction modeling (FIMoz), where the vertical displacement reflects faulting along a ∼34° dipping fault that extends to a depth of ∼35 km according to the data retrieved from the 2004 (M 6.2) Baladeh earthquake (Tatar et al., 2007; Donner et al., 2013). This model is driven by a regional present-day stress tensor with a N20°E directed S_{Hmax} (e.g., Landgraf et al., 2013 and references therein). Interestingly, the results show a positive spatial correlation between k_{sn} values and rock-uplift rates, corroborating the hypothesis that the k_{sn} pattern largely reflects thrusting along the Caspian Fault (Fig. 8).

The occurrence of localized, high k_{sn} values immediately upstream from the North Tehran Thrust suggests that fault reactivation may have occurred recently also along the southern flank (Fig. 5). For shortening rates of 1 mm/yr and a 30 to 45° dip angle of the North Tehran Thrust, uplift rates would be up to 0.07 to 0.2 mm/yr. However, the inferred low strain rates along the southern orogenic flank, the unknown pattern of faulting (e.g., Landgraf et al., 2009, 2013), and the possibility that GPS data do not effectively capture motion along a fault with long earthquake recurrence intervals, preclude us from estimating the spatial distribution rock uplift. In any case, exhumation rates derived from the linear inversion method over the last 3 Myr along the southern orogenic flank are significantly higher (0.5–0.6 mm/yr) than the estimated 0.07 to 0.2 mm/yr rock uplift rates (Fig. 8).

A significant southward shift in the drainage divide also appears to have occurred in this time frame. In the easternmost sectors of the Taleghan and Alamut intermontane basins (Fig. 2), external drainage with the development of large transverse river systems was triggered sometime during the last 3 Ma, as indicated by several ∼3 to 0.2 Ma incised lava flows capping undeformed Plio-Pleistocene gravels (Guest et al., 2007).

6. Discussion

We next explore the likely influences of tectonics, climate, and base-level fall on the orogenic evolution of the Alborz over each of the time intervals considered in the previous section. Following our interpretations for each time interval, we consider what factors have dominantly controlled changes in the orogenic architecture of the Alborz Mountains since ∼36 Ma.

6.1. Tectonic control on orogenesis between ∼36 to 6 Ma

The orographic barrier to moist air masses sourced in the Caspian Sea has existed at least since the onset of foreland-basin sedimentation at 17.5 Ma (Ballato et al., 2010). Despite this persistent, enhanced erosive potential on the northern flanks of the Alborz, rainfall patterns do not seem to have affected orogenic processes through the middle Miocene, as exhumation was focused along the southern mountain front until ca. 12 Ma (Figs. 3 and 4). Although short-term (10^5 yr) climatic variations recorded by stable isotope data along the southern flank appear to have contributed to temporary increases in sediment supply (Ballato and Strecker, 2014), it appears unlikely that those variations had a significant impact on the tectonic processes within the orogen, whose response time is generally considered to be an order of magnitude longer (Whipple and Meade, 2006; Whipple, 2009). The combination of southward (outward) orogenic growth, accelerated foreland-basin subsidence, enhanced sediment flux to the southern foreland, and decoupled precipitation and exhumation patterns suggests that from at least ∼18 to 9–6 Ma, tectonics exerted a first-order control on orogenic development.

6.2. Tectonic, climatic, and base-level control on orogenesis between 6 and 3 Ma

The shift in the locus of deformation to the northern orogenic front, together with the prominent increase in exhumation rates along the northern orogenic flank contrasting with a decrease along the southern flank between 6 and 3 Ma, marks a change in the architecture of the Alborz Mountains. The resulting pattern of deformation and exhumation can be used to test the likelihood of various climatic, tectonic, or base-level forcing mechanisms on orogenic evolution.

The potential influence of climate on these changes remains unclear due to the lack of local paleoclimatic data for that time interval. Paleoclimate reconstructions for the Mediterranean Sea suggest warm conditions with relatively high variability until ca. 5.5 Ma (e.g., Roveri et al., 2014), followed by less variable conditions until ∼3 Ma, when glaciations began to impact the northern hemisphere (e.g., Zachos et al., 2001). Overall, it seems unlikely that a less variable Pliocene (pre-3 Ma) climate could have forced the 6–3 Ma shift in the localization of fault-related exhumation across the range.

Alternatively, the changes in exhumation and deformation between ∼6 and 3 Ma might reflect a regional plate-tectonic reorganization associated with widespread deformation across the Arabian–Eurasian collision zone starting from ∼5 Ma (e.g., Axen et al., 2001; Allen et al., 2004; Guest et al., 2006b; Rezaeian et al., 2012). This mechanism, which was originally thought to be the cause for a renewed exhumation phase at 6–4 Ma in the Alborz mountains, however, does not explain why the locus of active deformation and exhumation shifted from the southern to the northern flank starting from 9–6 Ma.

A more compelling mechanism to trigger the change in structural architecture is the sudden, 0.6 to 1.5 km lowering of the Caspian Sea base level (Forte and Cowgill, 2013 and references therein) during its isolation from the Paratethys from ∼6 to 3.2 Ma, until a marine transgression re-established a connection with the Black Sea (e.g., Van Baak, et al., 2013). Observations from the Mediterranean region suggest that the rapid, km-scale base-level lowering event during the Messinian Salinity Crisis (e.g., Cosentino et al., 2013 and references therein) triggered a wave of river incision that propagated inland with a rate that varied as a function of drainage area (Loget and Van Den Driessche, 2009). Similar processes that occurred over a much longer time period promoted canyon incision in excess of 600 m depth through the shelf of the Caspian Sea and the Paleo-Mesozoic Russian Platform over a distance >1000 km from the present-day coastline (e.g., Forte and Cowgill, 2013 and references therein). Channel incision in turn would have increased the sediment flux from the adjacent hillslopes (e.g., Burbank, 2002) and routed that sediment into the Caspian Sea. Within the Alborz, our calculations of knickpoint celerity related to base-level fall indicate that large knickpoints that originated at ∼6 Ma would have been located at positions about 1/3 to half the length of present river profile, or at elevations between ∼500 and 1300 m (from E to W) with respect to the present sea-level at ∼3 Ma (Table 1; see also supplementary material). Thus, we interpret the prominent knickpoints that are currently at elevations of 1.5 to 2.4 km to be related to the base-level fall, as our celerity calculations suggest that 5 to 8 Myr are needed for migrating knickpoints to reach those locations (Table 1; Fig. 6; supplementary material). Overall, these calculations suggest that the prolonged base-level drop could have been associated with efficient mass-redistribution processes, especially along larger rivers experiencing high rock-uplift rates that drained the axial orogenic zone.

The onset of fluvial incision in the eastern sectors of the Taleghan and Alamut intermontane basins sometime during the

Table 1
Summary of knickpoint migration rates of rivers located along the northern flank of the central Alborz range (see Fig. 6 for channel location) and total response time for a base-level lowering, assuming that after 3 Myr erosion rates change from E1 to E2 (see Fig. 3). The position of the knickpoints after 3 Myr is also computed.

Channel	Knickpoint (KP) elevation [m]	Erosion rate 1 (E1) [mm/yrs]	Erosion rate 2 (E2) [mm/yrs]	Knickpoint after E1 [m]	Timing to present-day KP [Myr]	Total response time [Myr]
616	1267	0.35	0.4	983	3.7	5.2
616	1267	0.4	0.5	876	3.3	4.5
616	880	0.35	0.4	983	2.7	5.2
616	880	0.4	0.5	876	2.4	4.5
637	1077	0.35	0.4	956	3.3	7.5
637	1077	0.4	0.5	1114	2.9	6.3
660	2329**	0.35	0.4	984	6.5	8
660	2329**	0.4	0.5	1136	5.5	6.7
660	1583**	0.35	0.4	984	5	8
660	1583**	0.4	0.5	1136	4.3	6.7
660	914	0.35	0.4	984	2.8	8
660	914	0.4	0.5	1136	2.4	6.7
667	2411	0.35	0.4	993	6.6	7.9
667	2411	0.4	0.5	993	5.6	6.6
667	1029	0.35	0.4	1150	3.2	7.9
667	1029	0.4	0.5	1150	2.8	6.6
671	2157	0.35	0.45	996	5.6	7
671	2157	0.45	0.6	1298	4.5	5.5
671	1386**	0.35	0.45	996	3.8	7
671	1386**	0.45	0.6	1298	3.1	5.5
674	1710*	0.35	0.45	1000	4.5	7.7
674	1710*	0.45	0.6	1304	3.6	6
684	2122*	0.35	0.45	996	5.5	8.9
684	2122*	0.45	0.6	1303	4.4	6.9
691	3513	0.25	0.35	692	11.1	12.7
691	3513	0.35	0.5	992	8	9.2
691	2307**	0.25	0.35	692	7.6	12.7
691	2307**	0.35	0.5	992	5.6	9.2
691	930*	0.25	0.35	692	3.7	12.7
691	930*	0.35	0.5	925	2.8	9.2
694	1922	0.2	0.3	543	7.6	11.3
694	1922	0.3	0.5	829	5.2	7.4
698	2152*	0.2	0.3	543	8.6	10.5
698	2152*	0.3	0.5	829	5.8	6.9
698	1493**	0.2	0.3	543	6.3	10.5
698	1493**	0.3	0.5	829	4.4	6.9
702	2150*	0.2	0.3	543	8.5	11.9
702	2150*	0.3	0.5	829	5.7	7.7
707	1910**	0.2	0.3	535	7.8	10.8
707	1910**	0.3	0.5	828	5.3	7.1
714	1133	0.2	0.3	535	5.1	10.1
714	1133	0.3	0.5	828	3.7	6.7
724	1429*	0.2	0.3	551	5.9	8.9
724	1429*	0.3	0.5	846	4.2	5.9
733	1292	0.2	0.3	550	5.5	9.5
733	1292	0.3	0.5	845	3.9	6.3
735	2148	0.2	0.3	550	8.4	10.9
735	2148	0.3	0.5	854	5.6	7.1
740*	Equilibrium profile	0.2	0.3	527		8.8
740*	Equilibrium profile	0.3	0.5	826		5.9

* Knickpoints associated with a lithological contact (either fault or stratigraphic contact).
** Minor knickpoints.

last 3 Ma suggests that the capture of these basins should have started before 3 Ma. This event would have expanded the area draining to the Caspian Basin, producing a significant southward shift of the drainage divide and providing an additional source of sediments (Fig. 3). Although the causes responsible for the capture of these large intramontane basins are not clear, the prolonged ∼6 to 3.2 Ma base-level drop seems to be a viable mechanism.

In line with these inferences, from ∼6 to 3.2 Ma, the Caspian Sea received a significant volume of sediments from actively deforming mountain chains, including the Greater and Lesser Caucasus (Morton et al., 2003; Avdeev and Niemi, 2011), the Talesh Mountains (Madinapour et al. 2013), the Alborz Mountains (Axen et al., 2001; Guest et al., 2006a, 2006b), and possibly the Kopeh Dagh Mountains, as well as from stable regions including the Russian Platform, the Urals, and Central Asia (e.g., Reynolds et al., 1998; Morton et al., 2003; Abreu and Nummedal, 2007). The sedimentary sequences deposited in this time interval are known as the Productive Series (locally more than 6 km of sediments in less than then 3 Myr; e.g., Allen et al., 2002), a major hydrocarbon-reservoir unit composed of fluvio-deltaic sediments that grade basin-ward into turbidites (e.g., Reynolds et al., 1998; Brunet et al., 2003). Although the stratigraphic architecture of the Caspian Basin's southern margin is poorly known, studies have shown that a significant sediment supply was sourced from the Paleo-Kura, Paleo-Volga and Paleo-Amu Darya rivers (e.g., Reynolds et al., 1998; Abreu and Nummedal, 2007). In particular, heavy-mineral data from the western and northern margin of the South Caspian Basin indicate that the Caucasus were the dominant sediment source during the deposition of the Productive Series in

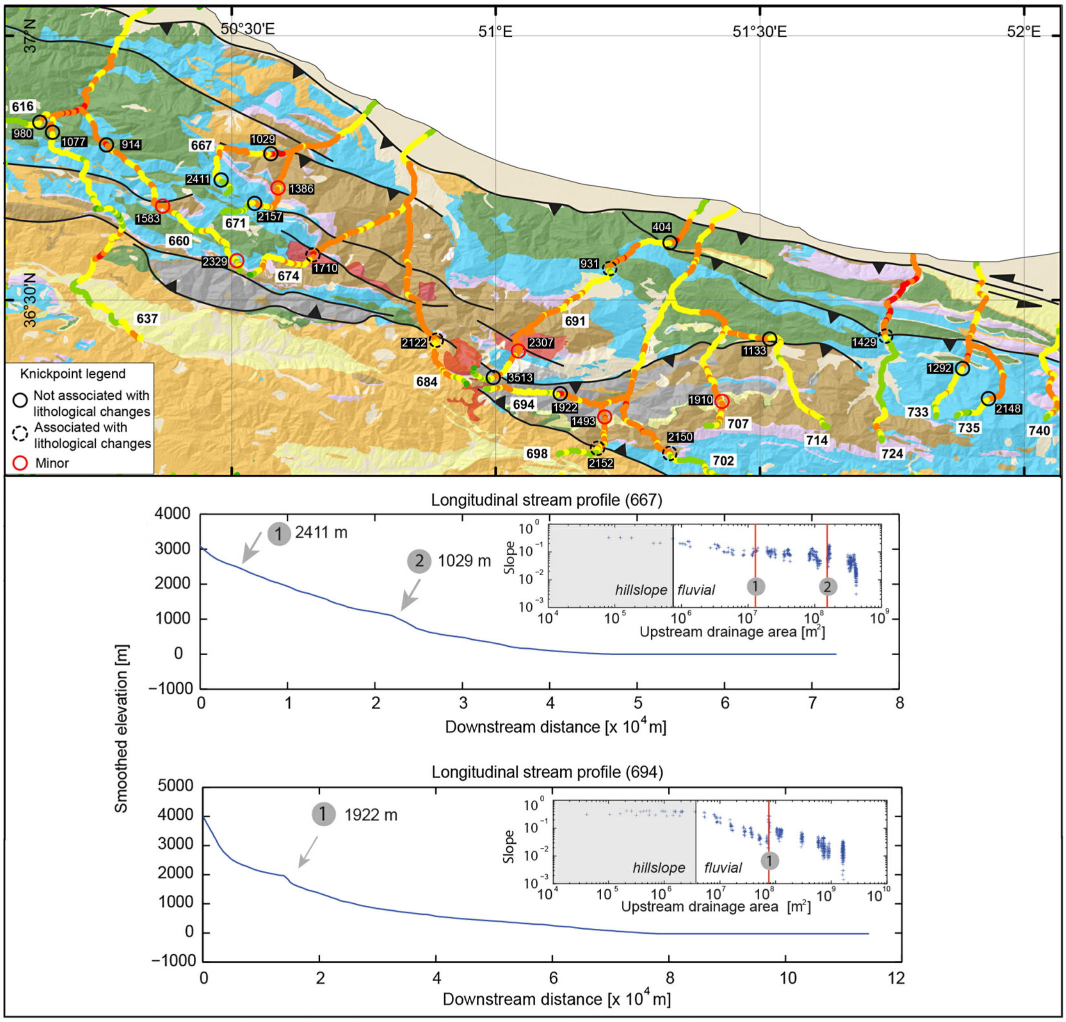

Fig. 6. Close up view of the northern flank of the Alborz Mountains (upper panel, see Fig. 2 for legend) with streams color-coded according to k_{sn} (see Fig. 5 for legend). The circles highlight the location of the knickpoints extracted from our channel steepness analysis, which is summarized on Table 1. The elevation of the knickpoints is shown in the black boxes while the stream codes are shown in the white boxes. The lower panel shows two representative river profiles and associated gradient versus upstream drainage area plotted on logarithmic scales. (For interpretation of the colors in this figure, the reader is referred to the web version of this article.)

the central–western Caspian Basin (Morton et al., 2003). Moreover, low-temperature thermochronology data from the Greater Caucasus, despite being scarce, are consistent with an influence from the Caspian base-level fall. In particular, the strong westward asymmetry of the drainage divide between the eastward and westward flowing rivers (to the Caspian and Black seas, respectively) could result from asymmetry in the efficiency of fluvial erosion processes associated with a shorter duration of the base level lowering event in the Black Sea with respect to the Caspian Sea (Krijgsman et al., 2010). Moreover, while exhumation rates in the east-draining sector of the Caucasus are about 0.75–1 mm/yr (averaged over the last ~5 Ma; Avdeev and Niemi, 2011; Avdeev, 2011), exhumation rates in west-draining sector are low (<0.1 mm/yr for the entire Cenozoic, Vincent et al., 2011). Therefore, although several mechanisms explaining the Pliocene exhumation and deformation patterns across the northern sectors of the Arabia–Eurasia collision zone have been proposed (see Austermann and Iaffaldano, 2013 and Forte et al., 2014 for a discussion), our observations raise the possibility that a base-level controlled, enhanced erosional phase may have contributed, through mass redistribution processes, to the inferred regional plate tectonic reorganization of the last ~5 Ma.

6.3. Partial coupling of climate and tectonics between 3 Ma and the present

Our modeling of the spatial distribution of rock uplift derived from geodetic shortening rates documents that the central–western sectors of the northern flank, which receive high precipitation and exhibit high k_{sn} values, are characterized by faster rock-uplift rates than the southern flank (Fig. 8). Considering that higher precipitation and hence potentially higher erosional efficiency favor a reduction in channel steepness, active tectonic deformation (most likely along the Caspian Fault) must be invoked to create such steep channels along the northern flank (e.g., Willett, 1999; Whipple, 2009). This configuration, with focused tectonic activity along the wetter northern flank, raises a major question: is there a positive feedback among orographically induced precipitation, focused exhumation, and rock uplift? The relatively good match between exhumation rates during the last 3 Ma and decadal erosion rates (Rezaeian, 2008), the spatial pattern of rock uplift inferred from river steepnesses, and our modelling of GPS-derived shortening rates and fault geometries suggest that once the northern flank of the orogen reached a lateral extent similar to the present one during the last 3 Myr, topographic steady state conditions were established (Fig. 8).

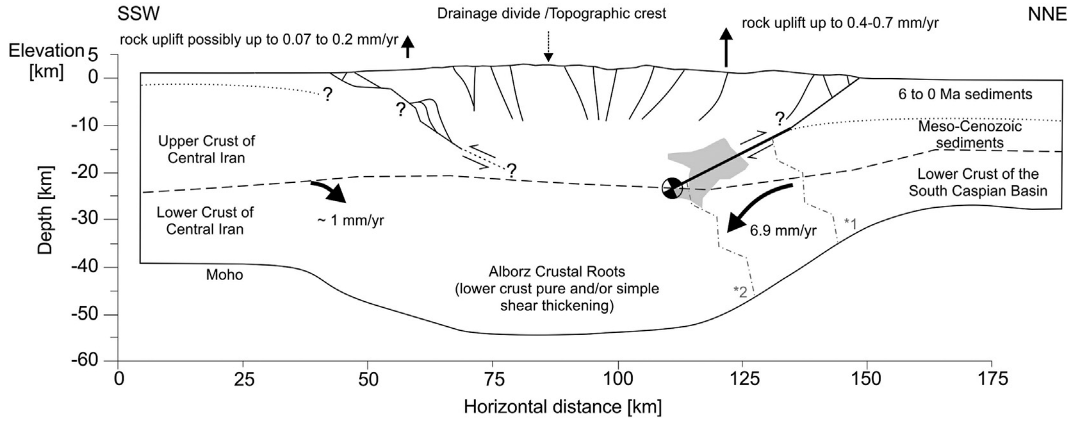

Fig. 7. Simplified crustal scale sketch approximately parallel to the swath profile S2 (see Fig. 5 for location). The crustal structure is from Motavalli-Anbaran et al. (2011). The earthquake focal mechanism for the 2004 Baladeh earthquake (M_w 6.2) and the location of main aftershocks (grey area) is from Donner et al. (2013). *1 and *2 represent the supposed location of the South Caspian lithosphere margin beneath the Alborz Mountains for 20 and 40 km of underthrusting. Uplift and underthrusting rates are extrapolated from GPS data assuming that Airy isostasy is approximately maintained, and for a 30 and 45° dip angle of the frontal faults along the northern and southern orogenic flank, respectively. Note that the Caspian Fault is supposed to juxtapose upper crustal rocks of the Alborz Mountains with thick marine sediments of the Caspian Sea at least at depths shallower than 13–11 km as suggested by the lack of shallow aftershocks, which is consistent with a thick pile of saturated overpressured sediments (Tatar et al., 2007).

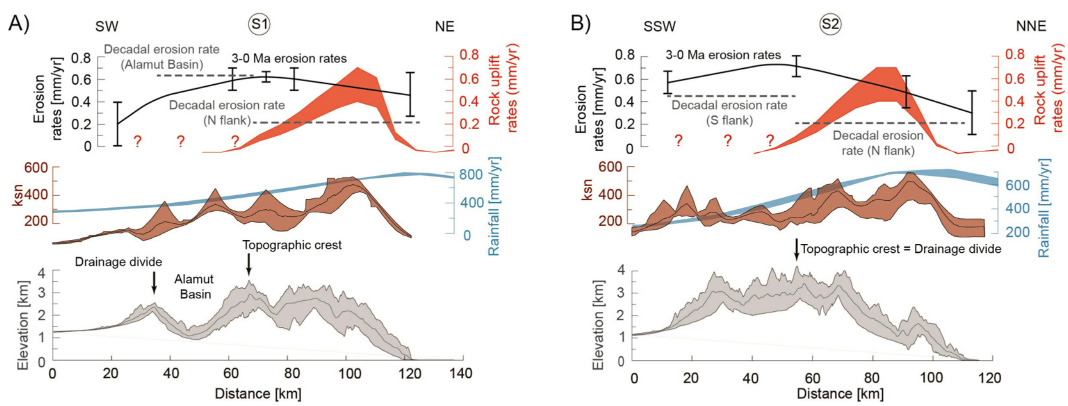

Fig. 8. Swaths profiles (see Fig. 5 for location) of topography (grey), rainfall (blue) and channel steepness indices (k_{sn}; pink) compared with GPS-inferred rock uplift rates (red), decadal erosion rates from suspended sediment concentrations measured at gauging stations (grey dashed line; Rezaeian, 2008), and erosion rates from the linear inverse calculation for the last 3 Ma (black line). The spatial distribution of rock uplift rates has been derived from the calculation of the vertical displacement field (see text for details). This approach is simplified and is used as a guideline for the present-day rock-uplift distribution associated with faulting along the Caspian Fault. (For interpretation of the references to color in this figure legend, the reader is referred to the web version of this article.)

This correlation between erosion and tectonically induced uplift, however, does not appear to exist along the drier southern orogenic flank, where slopes are also eroding fast despite experiencing low rainfall and low GPS-derived shorting and associated rock uplift rates (Fig. 8). While GPS-derived shortening rates may not be representative of long-term shortening rates, left-lateral wrenching dominates the modern deformation along the southern mountain front and in the Tehran plain (Ghassemi et al., 2014 and references therein). Although poorly constrained, such a kinematic changeover may have started between 3.2 and 4.7 Ma (Ghassemi et al., 2014), and hence could be well associated with our inferred change in the polarity of underthrusting. Moreover, while k_{sn} values immediately upstream from the hanging wall of the North Tehran Thrust are high, they are not as high as those in the hanging wall of the Caspian Fault (Figs. 5 and 8), supporting faster uplift of the northern flank compared to the south over million-year timescales. Even if we cannot accurately characterize rock uplift rates along the southern flank, the lack of correlation between rainfall patterns and exhumation rates across the orogen argues against a feedback among topography, tectonics, and climate at the scale of the entire orogen, implying that rainfall patterns have not modulated orogen-wide tectonic processes during the last 3 Myr.

6.4. Changes in the orogenic architecture of the Alborz Mountains

The lack of a positive orogen-scale feedback among tectonics and surface processes over the last 3 Ma, together with the observation that the southern flank has been eroding faster than the northern flank until the last 9–6 Ma (despite the presence of an orographic barrier to northerly winds since at least 17.5 Ma; Ballato et al., 2010), raise two additional questions. First, what caused the shift in the locus of active deformation and exhumation from the southern to the northern flank of the orogen, and second, what has controlled long-term orogenic processes in the Alborz Mountains?

A possible answer to these questions may reside in the modern crustal structure, which has resulted from crustal shortening (over 50 km; Guest et al., 2006b) and thickening (at least 15–20 km; e.g., Motavalli-Anbaran et al., 2011) processes over the last ∼36 Ma (Fig. 7). High exhumation rates along the southern flank, southward propagation of deformation fronts, development of a relatively deep southern foreland basin, incorporation of foreland-basin deposits into the orogenic wedge, and the occurrence of a rather stable, slowly advancing northern mountain front suggest that the tectonic accretionary flux, at least until the last 9 to 6 Ma, was focussed along the southern orogenic sectors. If true, during

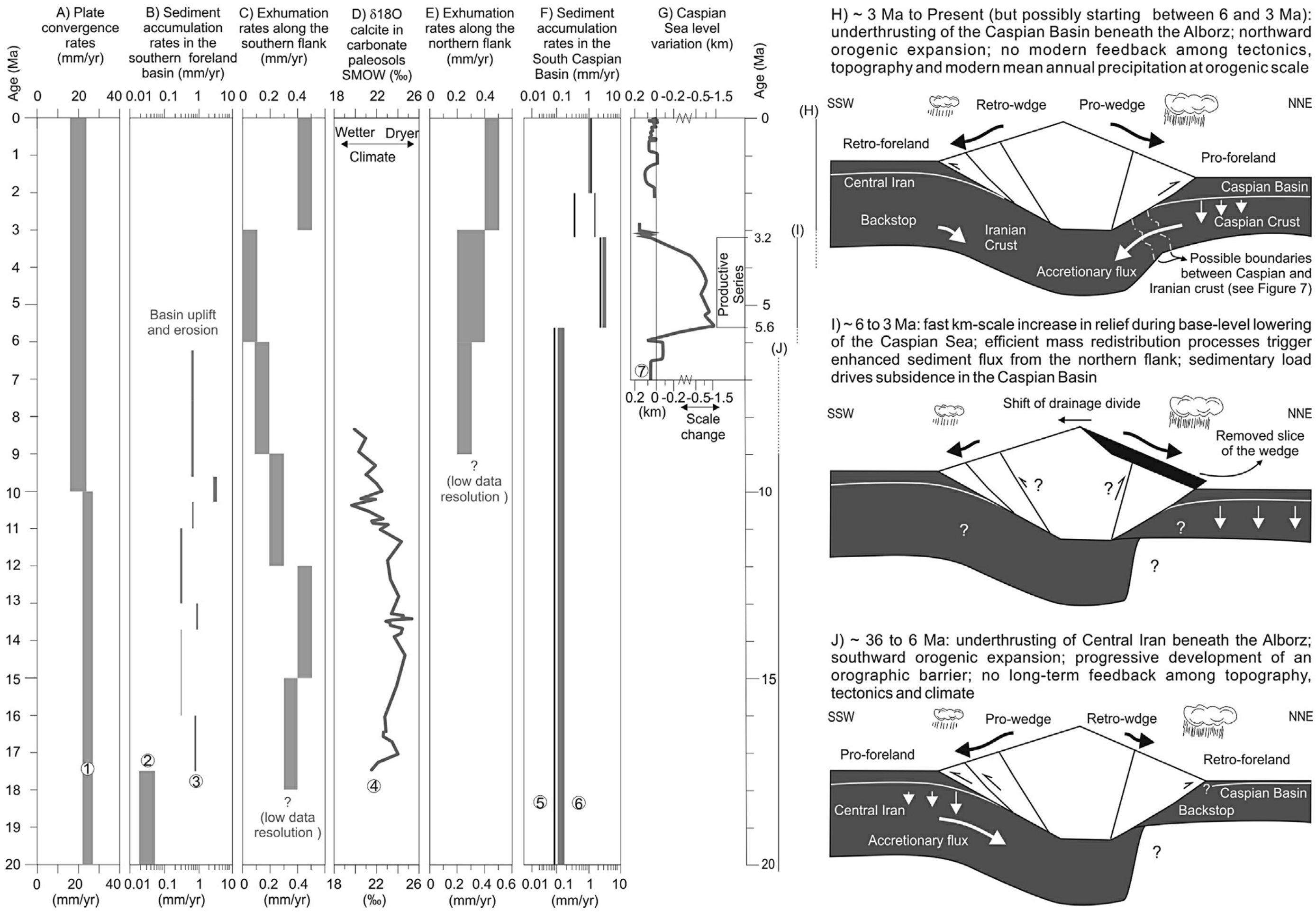

Fig. 9. Summary of the major tectono-stratigraphic events and paleoclimate data in the Alborz Mountains during the last 20 Ma. (A) Arabian–Eurasian plate convergence rates (McQuarrie et al., 2003), (B) sediment accumulation rates of the southern foreland basin (2: Ballato et al., 2011; 3: Ballato et al., 2008), (C) exhumation rates (this study), and (D) paleoclimate data (4: Ballato et al., 2010) for the southern orogenic flank. (E) Exhumation rates along the northern flank (this study), (F) sediment accumulation rates (5: Allen et al., 2002; 6: Brunet et al., 2003) and (G) eustatic sea curve of the South Caspian Basin for the last 6 Ma (7: Forte and Cowgill, 2013). (H to J) Evolutionary sketches, highlighting the 3 major orogenic stages recognized in this study.

the earliest stages of deformation, the southern mountain flank would have been the pro-wedge of the orogenic system, with Central Iran being underthrusted beneath the range, while the South Caspian Basin acted as backstop (Fig. 9). In light of these observations, the 9–6 Ma (or earlier) decrease in exhumation rates along the southern flank relative to the northern flank could reflect a decrease in the efficiency of underthrusting processes through the involvement of progressively thicker lithospheric sections of Central Iran in the deformation zone. However, this explanation remains speculative and requires further testing. Due to the paucity of deep geophysical data beneath the Alborz range, as well as the possible similarities between the lithosphere beneath Central Iran and the Alborz, we have few constraints on the deep orogenic structure, which precludes us from estimating the amount of underthrusting of Central Iran.

The subsequent mass redistribution triggered by the km-scale base-level fall of the Caspian Sea between ~6 and 3.2 Ma could have significantly changed the tectonic and geomorphic boundary conditions. Although lithospheric buckling (e.g., Brunet et al., 2003) and subduction of the south Caspian Basin beneath the central Caspian Basin (e.g., Allen et al., 2002) have been invoked as local subsidence mechanisms, sediment loading and compaction on a thermally subsiding late Mesozoic crust (either oceanic or highly thinned continental that developed as a back-arc basin in the Middle-Late Jurassic; e.g., Brunet et al., 2003; Motavalli-Anbaran et al., 2011) may account for the entire pattern of observed subsidence (Green et al., 2009). We suggest that the mass-redistribution processes triggered by the base-level fall and consequent increased sediment load in the basin may have ultimately caused the onset of northward subduction of the southern Caspian Basin beneath the central Caspian Basin, as well as the underthrusting of the South Caspian Basin beneath the Alborz Mountains. Although mechanisms behind the onset of subduction are a matter of debate (Stern et al., 2004), numerical and analytical solutions suggest that a cold, stiff continental margin characterized by fluid circulation, crustal-scale anisotropies, and a sedimentary load equivalent to ~10 km of thickness (like the Caspian Basin; Brunet et al., 2003) may be the locus of subduction initiation (Regenauer-Lieb et al., 2001). In our model, Central Iran became the new backstop of the orogenic system during the Pliocene, and a reversal in the direction of the accretionary flux occurred, focusing deformation along the northern flank in the new orogenic pro-wedge (Fig. 9), which is also (perhaps only coincidentally) the wetter orogenic side.

Underthrusting of the Caspian Basin is well documented by seismicity in the Talesh (Zanjani et al., 2013), the central Alborz (Tatar et al., 2007 and Donner et al., 2013), and the eastern Alborz (Nemati et al., 2013). It cannot have been established too long ago, because there is no geophysical evidence of deep subduction beneath the Alborz Mountains. If we extrapolate GPS-based underthrusting rates of ∼7 mm/yr over the last 6–3 Ma, the Caspian lithosphere should extend beneath the Alborz 40 to 20 km south of the northern thrust front (Fig. 7). This result is consistent with the presence of thickened crust at the northern flank as well as the pattern of seismicity at the interface between the underthrusting foreland lithosphere and the wedge.

We interpret these observations collectively to show that the southern orogenic flank evolved from a pro- to a retro-wedge (and vice versa for the northern flank), and that the underthrusting direction of the adjacent foreland lithosphere (Central Iran versus the South Caspian) has been the major driver of orogenesis in the Alborz Mountains (Fig. 9).

7. Conclusions

Based on our analysis of tectonic deformation, low-temperature thermochronology, and river profiles, we infer that the orogenic evolution of the Alborz Mountains has been primarily influenced by tectonic forcing and base-level changes. The spatiotemporal distribution of deformation, sedimentation, and exhumation prior to the late Miocene indicates focused deformation along the southern orogenic flank, most likely driven by north-directed underthrusting of the Central Iran lithosphere. As such, the development of the Alborz orogenic wedge appears to have been primarily influenced by tectonic processes until late Miocene time (sometime between 9 and 6 Ma). Subsequently, from ∼6 to 3 Ma, the km-scale (0.6 to 1.4 km) base-level fall in the Caspian Sea correlates with increased exhumation rates along the northern orogenic flank and decreased rates along the southern flank. This asymmetric exhumation can be explained by enhanced river incision triggered by the base-level fall, which in turn can explain the well documented regional increase in sediment flux into the Caspian Basin. This efficient mass redistribution, which presumably affected all the catchments draining to the Caspian Basin, caused significant basin subsidence, which may have ultimately influenced the regional tectonics. Specifically, we speculate that rapid sediment loading and subsidence triggered the southward underthrusting of the Caspian Basin beneath the Alborz Mountains and possibly northward subduction beneath the Central Caspian region. Deformation subsequently became focused along the wetter northern orogenic flank, which experienced renewed outward expansion, becoming the new pro-wedge of the orogenic system during the last 3 Myr. The coincidence in the locus of active shortening and rainfall maximum led to the establishment of topographic steady-state conditions along the northern orogenic flank, but it did not result in a climatically controlled tectonic regime at the scale of the entire orogen, as documented by the spatially decoupled patterns of rainfall, rock uplift, exhumation during the last 3 Ma, and decadal erosion rates along the southern flank of the range.

Acknowledgements

P.B. and A.L. were funded by the German Science Foundation (DFG STR 373/19-1 and DFG BA 4420/2-1), the graduate school program of the University of Potsdam (DFG STR 373/18-1), and the Leibniz Center of Surface Process Studies and Climate Geology (DFG STR 373/15-1) granted to M.R.S. T.S. was funded by the German Science Foundation (DFG SCHI 1241/1-1 granted to T.S.). The Building and Housing Research Center of Tehran and the Geological Survey of Tehran are thanked for providing logistical support. We thank R. Thiede (U Potsdam) for helpful comments on the manuscript, B. Bookhagen for rainfall data, and T. Roeper for sample preparation. We are grateful to B. Ghorbal, R. Kislitsyn, S. Brichau and students of the (U–Th)/He laboratory at the University of Kansas for providing technical support. We also acknowledge the Editor An Yin and constructive revisions provided by P. van der Beek and A. Forte.

Appendix A. Supplementary material

Supplementary material related to this article can be found online at http://dx.doi.org/10.1016/j.epsl.2015.05.051.

References

Abreu, V., Nummedal, D., 2007. Miocene to Quaternary sequence stratigraphy of the South and Central Caspian basins. In: Yilmaz, P.O., Isaksen, G.H. (Eds.), Oil and Gas of the Greater Caspian Area. In: AAPG Stud. Geol., vol. 55, pp. 65–86.
Allen, M., Ghassemi, M.R., Shahrabi, M., Qorashi, M., 2003. Accommodation of late Cenozoic oblique shortening in the Alborz range, northern Iran. J. Struct. Geol. 25, 659–672.
Allen, M.B., Jones, S., Ismail-Zadeh, A.D., Simmons, M.D., Anderson, L., 2002. Onset of subduction as the cause of rapid Pliocene/Quaternary subsidence in the South Caspian basin. Geology 30, 775–778.
Allen, M., Jackson, J., Walker, R., 2004. Late Cenozoic reorganization of the Arabia–Eurasia collision and the comparison of short-term and long-term deformation rates. Tectonics 23, TC2008.
Austermann, J., Iaffaldano, G., 2013. The role of the Zagros orogeny in slowing down Arabia–Eurasia convergence since ∼5 Ma. Tectonics 32, TC20027.
Avdeev, B., 2011. Tectonics of the Greater Caucasus and the Arabia–Eurasia Orogen. Ph.D. thesis. University of Michigan, Ann Arbor, 137 pp.
Avdeev, B., Niemi, N.A., 2011. Rapid Pliocene exhumation of the central Greater Caucasus constrained by low-temperature thermochronometry. Tectonics 30, TC2009.
Axen, G.J., Lam, P.J., Grove, M., Stockli, D.F., Hassanzadeh, J., 2001. Exhumation of the west-central Alborz mountains, Iran, Caspian subsidence, and collision-related tectonics. Geology 29, 559–562.
Ballato, P., Strecker, M.R., 2014. Assessing tectonic and climatic causal mechanisms in foreland-basin stratal architecture: insights from the Alborz Mountains, northern Iran. Earth Surf. Process. Landf. 39, 110–125.
Ballato, P., Nowaczyk, N.R, Landgraf, A., Strecker, M.R., Friedrich, A., Tabatabaei, S.H., 2008. Tectonic control on sedimentary facies pattern and sediment accumulation rates in the Miocene foreland basin of the southern Alborz mountains, northern Iran. Tectonics 27, TC6001.
Ballato, P., Mulch, A., Landgraf, A., Strecker, M.R., Dalconi, M.C., Friedrich, A., Tabatabaei, S.H., 2010. Middle to Late Miocene Middle Eastern climate from stable oxygen and carbon isotope data, southern Alborz mountains, N Iran. Earth Planet. Sci. Lett. 300, 125–138.
Ballato, P., Uba, C.E., Landgraf, A., Strecker, M.R., Sudo, M., Stockli, D.F., Friedrich, A., Tabatabaei, S.H., 2011. Arabia–Eurasia continental collision: insights from late Tertiary foreland-basin evolution in the Alborz mountains, northern Iran. Geol. Soc. Am. Bull. 123, 106–131.
Ballato, P., Stockli, D.F., Ghassemi, M.R., Landgraf, A., Strecker, M.R., Hassanzadeh, J., Friedrich, A., Tabatabei, S.H., 2013. Accommodation of transpressional strain in the Arabia–Eurasia collision zone: new constraints from (U–Th)/He thermochronology in the Alborz Mountains, N Iran. Tectonics 32, TC003159.
Berberian, M., 1983. The Southern Caspian: a compressional depression floored by a trapped, modified oceanic crust. Can. J. Earth Sci. 20, 163–183.
Bookhagen, B., Strecker, M.R., 2012. Spatiotemporal trends in erosion rates across a pronounced rainfall gradient: examples from the southern Central Andes. Earth Planet. Sci. Lett. 327/328, 97–110.
Brunet, M.F., Korotaev, M.V., Ershov, A.V., Nikishin, A.M., 2003. The South Caspian Basin: a review of its evolution from subsidence modeling. Sediment. Geol. 156, 119–148.
Burbank, D.W., 2002. Rates of erosion and their implications for exhumation. Mineral. Mag. 66, 25–52.
Burbank, D.W., Blythe, A.E., Putkonen, J., Pratt-Sitaula, B., Gabet, E., Oskin, M., Barros, A., Ojha, T.P., 2003. Decoupling of erosion and precipitation in the Himalayas. Nature 426, 652–655.
Cosentino, D., Buchwaldt, R., Sampalmieri, G., Iadanza, A., Cipollari, P., Schildgen, T.F., Hinnov, L.A., Ramezani, J., Bowring, S.A., 2013. Refining the Mediterranean "Messinian gap" with high-precision U–Pb zircon geochronology, central and northern Italy. Geology 41, 323–326.
Davidson, J., Hassanzadeh, J., Berzins, R., Stockli, D.F., Bashukooh, B., Turrin, B., Pandamouz, A., 2004. The geology of Damavand volcano, Alborz Mountains, northern Iran. Geol. Soc. Am. Bull. 116, 16–29.
Davis, D., Suppe, J., Dahlen, F.A., 1983. Mechanics of fold-and-thrust belts and accretionary wedges. J. Geophys. Res. 88, 1153–1172.
DiBiase, R.A., Whipple, K.X., 2011. The influence of erosion thresholds and runoff variability on the relationships among topography, climate, and erosion rate. J. Geophys. Res. 116, F04036.
Djamour, Y., Vernant, P., Bayer, R., Nankali, H., Ritz, J.F., Hinderer, J., Hatam, Y., Luck, B., Le Moigne, N., Sedighi, M., Khorramiet, et al., 2010. GPS and gravity

constraints on continental deformation in the Alborz mountain range, Iran. Geophys. J. Int. 183, 1287–1301.
Donner, S., Rößler, D., Krüger, F., Ghods, A., Strecker, M.R., 2013. Segmented seismicity of the Mw 6.2 Baladeh earthquake sequence (Alborz mountains, Iran) revealed from regional moment tensors. J. Seismol. 17, 925–959.
Farley, K., 2000. Helium diffusion from apatite; general behavior as illustrated by Durango fluorapatite. J. Geophys. Res. 105, 2903–2914.
Farley, K.A., Wolf, R.W., Silver, L.T., 1996. The effects of long alpha-stopping distances on (U–Th)/He ages. Geochim. Cosmochim. Acta 60, 4223–4229.
Forte, A.M., Cowgill, E., 2013. Late Cenozoic base-level variations of the Caspian Sea: a review of its history and proposed driving mechanisms. Palaeogeogr. Palaeoclimatol. Palaeoecol. 386, 392–407.
Forte, A.M., Cowgill, E., Whipple, K.X., 2014. Transition from a singly vergent to doubly vergent wedge in a young orogen: the Greater Caucasus. Tectonics 33, 2077–2101.
Fox, M., Herman, F., Willett, S.D., May, D.A., 2014. A linear inversion method to infer exhumation rates in space and time for thermochronometric data. Earth Surf. Dyn. 2, 47–85.
Gasparini, N., Whipple, K.W., 2014. Diagnosing climatic and tectonic controls on topography: Eastern flank of the Northern Bolivian Andes. Lithosphere 6, 230–250.
Ghassemi, M.R., 2005. Drainage evolution in response to fold growth in the hanging-wall of the Khazar fault, north-eastern Alborz, Iran. Basin Res. 17, 425–436.
Ghassemi, M.R., Fattahi, M., Landgraf, A., Ahmadi, M., Ballato, P., Tabatabaei, S.H., 2014. Kinematic links between the Eastern Mosha Fault and the North Tehran Fault, Alborz Range, northern Iran. Tectonophysics 622, 81–95.
Green, T., Abdullayev, N.R., Hossack, J., Riley, G., Roberts, A.M., 2009. Sedimentation and subsidence in the South Caspian Basin, Azerbaijan. Geol. Soc. (Lond.) Spec. Publ. 312, 241–260.
Guest, B., Axen, G.J., Lam, P.S., Hassanzadeh, J., 2006a. Late Cenozoic shortening in the westcentral Alborz mountains, northern Iran, by combined conjugate strike-slip and thin-skinned deformation. Geosphere 2, 35–52.
Guest, B., Stockli, D.F., Grove, M., Axen, G.J., Lam, P.S., Hassanzadeh, J., 2006b. Thermal histories from the central Alborz mountains, northern Iran: implications for the spatial and temporal distribution of deformation in northern Iran. Geol. Soc. Am. Bull. 118, 1507–1521.
Guest, B., Horton, B.K., Axen, G.J., Hassanzadeh, J., McIntosh, W.C., 2007. Middle to late Cenozoic basin evolution in the western Alborz Mountains: implications for the onset of collisional deformation in northern Iran. Tectonics 26, TC6011.
Hodges, K., Wobus, C.W., Ruhl, K., Schildgen, T., Whipple, K., 2004. Quaternary deformation, river steepening, and heavy precipitation at the front of the Higher Himalayan ranges. Earth Planet. Sci. Lett. 220, 379–389.
Hoth, S., Adam, J., Kukowshi, N., Oncken, O., 2006. Influence of erosion on the kinematics of bivergent orogens: results from scaled sandbox simulation. In: Willett, S.D., Hovius, N., Brandon, M., Fisher, D.M. (Eds.), Tectonics, Climate, and Landscape Evolution. In: Geological Society of America Special Paper, vol. 398, pp. 201–225.
Javanmard, S., Yagatai, A., Nodzu, M.I., Bodagh Jamali, J., Kawamoto, H., 2010. Comparing high-resolution gridded precipitation data with satellite rainfall estimates of TRMM 2B42 over Iran. Adv. Geosci. 25, 119–125.
Kirby, E., Whipple, K.X., 2012. Expression of active tectonics in erosional landscapes. J. Struct. Geol. 44, 54–75.
Koons, P.O., 1990. The two-sided orogen: collision and erosion from the sand box to the Southern Alps, New Zealand. Geology 18, 679–682.
Krijgsman, W., Stoica, M., Vasiliev, I., Popov, V.V., 2010. Rise and fall of the Paratethys Sea during the Messinian Salinity Crisis. Earth Planet. Sci. Lett. 290, 183–191.
Landgraf, A., Ballato, P., Strecker, M.R., Friedrich, A., Tabatabaei, S.H., Shahpasandzadeh, M., 2009. Fault-kinematic and geomorphic observations along the North Tehran Thrust and Mosha Fasham Fault, Alborz mountains, Iran: implications for fault-system evolution and interaction in a changing tectonic regime. Geophys. J. Int. 177, 676–690.
Landgraf, A., Zielke, O., Arrowsmith, R., Ballato, P., Strecker, M.R., Schildgen, T.F., Friedrich, A., Tabatabaei, S.H., 2013. Differentiating simple and composite tectonic landscapes using numerical fault-slip modeling with an example from the south-central Alborz Mountains. J. Geophys. Res., Earth Surf. 118, 1792–1805.
Loget, N., Van den Driessche, J., 2009. Wave train model for knickpoint migration. Geomorphology 106, 376–382.
Madanipour, S., et al., 2013. Synchronous deformation on orogenic plateau margins: insights from the Arabia–Eurasia collision. Tectonophysics 608, 440–451.
McQuarrie, N., Stock, J.M., Verdel, C., Wernicke, B.P., 2003. Cenozoic evolution of Neotethys and implications for the causes of plate motions. Geophys. Res. Lett. 30, 2036.
Morton, A., et al., 2003. Provenance patternes in a neotectonic basin: Pliocene and Quaternary sediment supply to the South Caspian. Basin Res. 15, 321–337.
Motavalli-Anbaran, S.H., Zeyen, H., Brunet, M.F., Ardestani, V.E., 2011. Crustal and lithospheric structure of the Alborz Mountains, Iran, and surrounding areas from integrated Geophysical modeling. Tectonics 30, TC5012.
Nemati, M., Hollingsworth, J., Zhong, W., Bolourchi, M.J., Talebian, M., 2013. Microseismicity and seismotectonics of the South Caspian Lowlands, northeast of Iran. Geophys. J. Int. 193, 1053–1070.
Regenauer-Lieb, K., Yuen, D.A., Branlund, J., 2001. The initiation of subduction: criticality by addition of water? Science 294, 578–580.
Reiners, P.W., Brandon, M.T., 2006. Using thermochronology to understand orogenic erosion. Annu. Rev. Earth Planet. Sci. 34, 419–466.
Reynolds, A.D., et al., 1998. Implications of outcrop geology for reservoirs in the Neogene productive series; Aspheron Peninsula, Azerbaijan. AAPG Bull. 82, 25–49.
Rezaeian, M., 2008. Coupled tectonics, erosion and climate in the Alborz Mountains. Ph.D. thesis. University of Cambridge, Cambridge, UK. 237 pp.
Rezaeian, M., Carter, A., Hovius, N., Allen, M.B., 2012. Cenozoic exhumation history of the Alborz Mountains, Iran: new constraints from low-temperature chronometry. Tectonics 31, TC2004.
Roveri, M., Flecker, R., Krijgsman, W., Lofi, J., Lugli, S., Manzi, V., Sierro, J.S., Bertini, A., Carmelenghi, A., De Lange, G., Govers, R., Hilgen, F.J., Hübscher, C., Meijer, P.T., Stoica, M., 2014. The Messinian Salinity Crisis: past and future of a great challenge for marine sciences. Mar. Geol. 352, 25–58.
Sass, J.H., Lachenbruch, A.H., Munroe, J., 1971. Thermal conductivity of rocks from measurements on fragments and its application to heat-flow determinations. J. Geophys. Res. 76, 3391–3401.
Stern, R.J., 2004. Subduction initiation: spontaneous and induced. Earth Planet. Sci. Lett. 226, 275–292.
Tatar, M., Jackson, J., Hatzfeld, D., Bergman, E., 2007. The 2004 May 28 Baladeh earthquake (Mw 6.2) in the Alborz, Iran: overthrusting the South Caspian Basin margin, partitioning of oblique convergence and the seismic hazard of Tehran. Geophys. J. Int. 170, 249–261.
Thiede, R.C., et al., 2004. Climatic control on rapid exhumation along the Southern Himalayan Front. Earth Planet. Sci. Lett. 222, 791–806.
Van Baak, C.G.C., et al., 2013. A magnetostratigraphic time frame for Plio-Pleistocene transgressions in the South Caspian Basin, Azerbaijan. Glob. Planet. Change 103, 119–134.
Vincent, S.J., Carter, A., Lavrishchev, A., Rice, S.P., Barabadze, T.G., Hovius, N., 2011. The exhumation of the western Greater Caucasus: a thermochronometric study. Geol. Mag. 148, 1–21.
Whipple, K.X., 2009. The influence on climate on the tectonic evolution of mountain belts. Nat. Geosci. 2, 97–104.
Whipple, K.X., Meade, B.J., 2006. Orogen response to changes in climatic and tectonic forcing. Earth Planet. Sci. Lett. 243, 218–228.
Whipple, K.X., Tucker, G.E., 1999. Dynamics of the stream-power river incision model: implications for height limits of mountain ranges, landscape response timescales, and research needs. J. Geophys. Res. 104, 17661–17674.
Willett, S.D., 1999. Orogeny and orography: the effects of erosion on the structure of mountain belts. J. Geophys. Res. 104, 28957–28981.
Willett, S., Beaumont, C., Fullsack, P., 1993. Mechanical models for the tectonics of doubly vergent compressional orogens. Geology 21, 371–374.
Wobus, C., Whipple, K.X., Kirby, E., Snyder, N., Johnson, N., Spyropolou, K., Crosby, B., Sheehan, D., 2006. Tectonics from topography: procedures, promise, and pitfalls. In: Willett, S.D., Hovius, N., Brandon, M.T., Fisher, D.M. (Eds.), Tectonics, Climate, and Landscape Evolution. In: Geological Society of America Special Paper, vol. 398, pp. 55–74.
Wolfe, M.R., Stockli, D.F., 2010. Zircon (U–Th)/He thermochronometry in the KTB drill hole, Germany, and its implications for bulk He diffusion in zircon. Earth Planet. Sci. Lett. 295, 69–82.
Zachos, J., Pagani, M., Sloan, L., Thomas, E., Billups, K., 2001. Trends, rhythms, and aberrations in global climate 65 Ma to present. Science 292, 686–693.
Zanchi, A., Berra, F., Mattei, M., Ghassemi, M.R., Sabouri, J., 2006. Inversion tectonics in central Alborz, Iran. J. Struct. Geol. 28, 2023–2037.
Zanjani, A.A., Ghods, A., Sobouti, F., Bergman, E., Mortezanejad, G., Priestley, K., Madanipour, S., Rezaeian, M., 2013. Seismicity in the western coast of the South Caspian Basin and the Talesh Mountains. Geophys. J. Int. 195, 799–814.